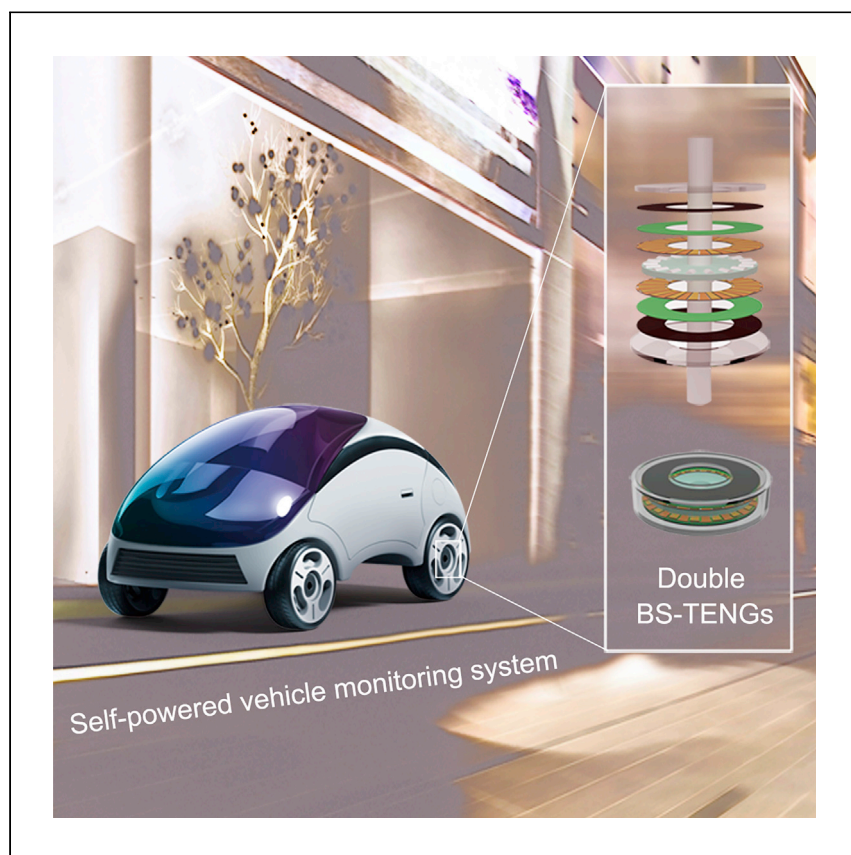


Article

3D-printed bearing structural triboelectric nanogenerator for intelligent vehicle monitoring



In order to upgrade the working frequency, Yang et al. fabricate a bearing structural triboelectric nanogenerator (BS-TENG) with a maximum of 1,500 rpm by 3D printing, which enables a higher working frequency. This BS-TENG unit delivers a peak power of 0.96 mW and can be successfully integrated into a self-powered vehicle monitoring system.

Jin Yang, Yanshuo Sun, Jianjun Zhang, Baodong Chen, Zhong Lin Wang

chenbaodong@binn.cas.cn (B.C.)
zlwang@gatech.edu (Z.L.W.)

Highlights

The speed of 3D printed bearing structure triboelectric nanogenerator reaches 1,500 rpm

One unit delivers a peak power of 0.96 mW

It only takes about 80 s to charge a capacitor of 1000 μ F to 4 V

The accuracy of the self-powered vehicle speed monitoring could be more than 99%

Article

3D-printed bearing structural triboelectric nanogenerator for intelligent vehicle monitoring

Jin Yang,^{1,2} Yanshuo Sun,^{1,2} Jianjun Zhang,^{1,2} Baodong Chen,^{1,3,4,7,*} and Zhong Lin Wang^{1,3,5,6,*}

SUMMARY

Maintaining a high working frequency is one of the critical technical solutions to the triboelectric nanogenerator (TENG) for improving its output power. Herein, we propose a bearing structural TENG (BS-TENG), which achieves a speed of nearly 1,500 rpm based on the diversified design of 3D printing. It is vital that a BS-TENG unit delivers a peak power of 0.96 mW under an external load of 8 M Ω and, in addition, charges a capacitor of 1,000 μ F to reach a voltage of 4 V that takes merely 80 s at a rotational speed of 600 rpm. The integrated BS-TENG network serves as both an energy harvester and a self-powered high-speed sensing system for the safe operation of vehicles. This study presents an approach for upgrading the working frequency of TENGs and may provide new opportunities for TENGs in intelligent automobile driving systems.

INTRODUCTION

With the rapid development of science and technology, automated vehicle and artificial intelligence fields have developed rapidly over the past few decades^{1,2} and are facing unprecedented challenges in their sustainable energies and supply ways. In fact, it turns out that the unreasonable energy supply patterns and energy structures lead to the current development dilemma. On the one hand, large-scale signal processing systems and sensor networks are being widely applied in autonomous vehicles to ensure completely safe and reliable driving, which have resulted in higher demands for a power source and its supply modes.^{3,4} In addition, a series of accessory equipment has to be added in order for the system to run normally. Existing prominent problems include frequent charging and its slow process and extremely complex wired networks, etc., which inevitably lead to increased manufacturing costs, potential safety hazards, and complexity.⁵ Besides, comprehensive advantages of a light weight, flexibility, miniaturization, and portability are needed. However, the traditional centralized and ordered energy supply patterns based on power plants are incompatible with the present development of distributed energy and wireless and portable electronic devices. Although energy storage devices, such as super-capacitors and each kind of battery, have had rapid development in recent decades, there are questions about the need for them to be replaced regularly, their frequent charging, causing irreversible environmental damage, and so on.^{6,7} A huge amount of rotating mechanical energy will inevitably be generated during vehicle driving and braking, but it is completely ignored due to limited existing energy conversion technologies. Thus, an innovative harvesting technology is required to convert the wasted rotating mechanical energy into electricity in order to achieve a self-powered sensing system for autonomous vehicles.^{8–11}

Therefore, from long-term development objectives and environmental perspectives, power acquisition directly from the natural environment is the ideal choice

¹Beijing Institute of Nanoenergy and Nanosystems, Chinese Academy of Sciences, Beijing 101400, P.R. China

²College of Chemistry and Chemical Engineering, Center on Nanoenergy Research, Guangxi University, Nanning, 530004, P.R. China

³School of Nanoscience and Technology, University of Chinese Academy of Sciences, Beijing 100049, P.R. China

⁴Institute of Applied Nanotechnology, Jiaxing, Zhejiang 314031, P.R. China

⁵CUSTech Institute, Wenzhou, Zhejiang 325024, P.R. China

⁶School of Materials Science and Engineering, Georgia Institute of Technology, Atlanta, GA 30332-0245, USA

⁷Lead contact

*Correspondence:
chenbaodong@binn.cas.cn (B.C.),
zlwang@gatech.edu (Z.L.W.)

<https://doi.org/10.1016/j.xcrp.2021.100666>

for future energy supplies. This idea was first proposed by Z.L. Wang in 2006¹², when he invented the nanogenerator (NG), and then he also invented the triboelectric nanogenerator (TENG), which is a revolutionary energy harvesting technology that stands out from the rest with its own advantages and stand-out features, in 2012¹³. Previous research has shown that the rotary-sliding-structured TENGs have been widely used to harvest mechanical energy from wind and the rotation of the wheels.^{14–18} Meanwhile, self-powered sensing technology based on TENGs has been greatly developed due to its advantages over traditional power supply technology.^{19,20} Even so, the development of TENGs for real-time power supply, high-speed rotation, and special structure is still hindered because of the exacting requirements of autonomous vehicles. The great thing is that various 3D-printed TENG devices used in specific scenarios have been researched with the rapid development and maturity of 3D-printed technology.^{21–25} In a nutshell, it is meaningful to design new structures of TENGs to achieve rotational energy harvesting and a self-powered sensing system for the safer driving of automated vehicles.

In this work, we use 3D printing to fabricate an entirely new bearing structural TENG (BS-TENG), which can serve as both a rotational mechanical energy harvester and a self-powered sensor system under the high rotational speed range. The operating speed of BS-TENG can reach a maximum of approximately 1,500 rpm by polytetrafluoroethylene (PTFE) rollers and 3D printing diversified structure design, in which one unit delivers a peak power of 0.96 mW under an external load of 8 M Ω . In addition, a self-powered vehicle-sensing system includes a high rotational speed sensor composed of one unit and an energy-harvesting network consisting of seven units, which is capable of real-time monitoring local temperature and vehicle speed. The energy-harvesting network can deliver a short-circuit current of 76 μ A, an open-circuit voltage of 80 V, and the transferred charges of 85 nC under the rotational speed of 900 rpm. Moreover, it takes about 80 s to charge a capacitor of 1,000 μ F by the energy-harvesting network to achieve a voltage of 4 V under a rotational speed of 600 rpm. Compared with TENGs of similar size, the charging efficiency of BS-TENG has been increased by nearly 5 times. This breakthrough is due to the novel structural design and optimization of BS-TENGs. It could also directly light up 50 series commercial light-emitting diodes (LEDs) and an electronic thermometer. Additionally, findings reveal that the working frequency of the BS-TENG accurately change with the increase of rotational speed, showing its potential application as a self-powered speed sensor. The accuracy exceeds 99% level under a wide speed range of 100 to 1,500 rpm. This new approach is a potential solution to harvesting high-speed and wasted rotating mechanical energy. It also upgrades the operating speed of TENG to a new height.

RESULTS

Structure and working principle of BS-TENG

As one of the most important modes of transportation in the future, the automated vehicle, with the advantages of intelligence, good safety, and precise positioning, is popular with drivers. These advantages benefit from the cooperation of a large number of sensors, which require huge amounts of energy and manufacturing costs. Simultaneously, rotational energy generated by the movement of the automated vehicle is completely wasted. Therefore, the BS-TENG is obtained by 3D printing, which can run stably at a high speed: up to 1,500 revolutions per minute. Furthermore, eight generators are integrated into a self-powered vehicle monitoring (SPVM) system. The system, with the dual functions of harvesting rotational energy and sensing, is concentrically fixed on a principal axis, which makes it work

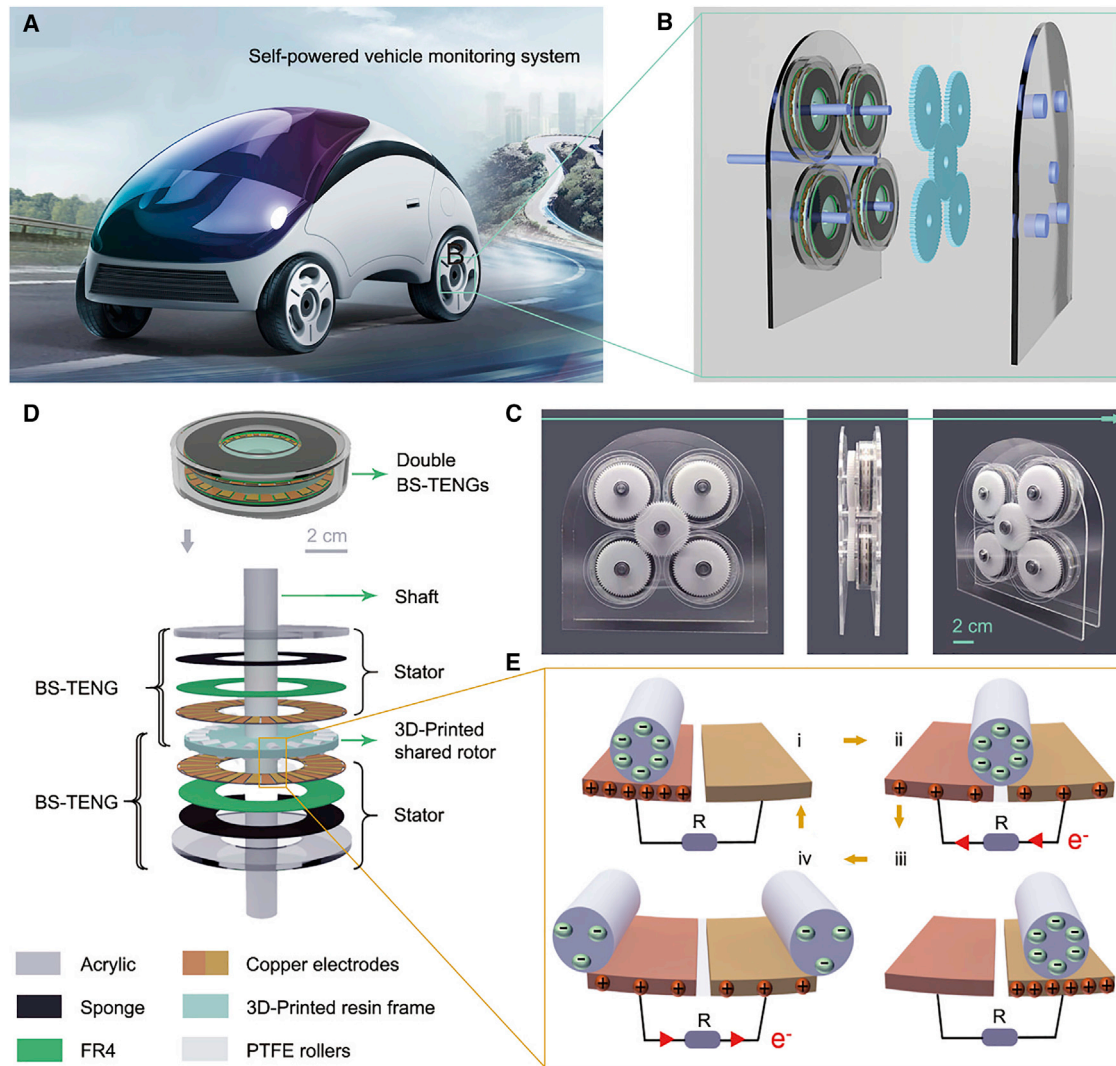


Figure 1. Structural design and working mechanism of BS-TENG

- (A) Self-powered vehicle monitoring system fixed on principal axis of automated vehicle.
 (B) Schematic illustration of self-powered vehicle monitoring system based on eight BS-TENG units applied on autonomous vehicles.
 (C) Photographs of the system from different views.
 (D) Schematic representation of the structure of the double BS-TENGs.
 (E) Schematic working principle of BS-TENG with rolling-type free-standing mode.

synchronously with principal axis rotating. The application scenario is visualized in Figure 1A. The SPVM-system is mainly composed of four double-BS-TENGs, five gears, and two acrylic plates, which are detailed in the breakdown structure diagram that can be seen in Figure 1B. For a more intuitive observation, different perspective photographs of the SPVM-system are illustrated in Figure 1C. BS-TENG, which adopted a freestanding mode and is packaged in an acrylic tube, is composed of a shared 3D-printed rotor and a stator. The detailed breakdown structure of double-BS-TENGs is shown in Figure 1D. The rotor element includes PTFE rollers as negative layers and a 3D-printed resin frame. A 3D-printed shared rotor with roller interspaces (length of 9 mm), which are left to fill the PTFE rollers, is the key idea of this design. As a positive layer, the copper (Cu) electrode disk with two groups of complementary grating electrodes was fabricated utilizing printed circuit board

(PCB) technology, which is adhered to a piece of sponge and further attached to a circular acrylic plate, creating the stator element. Two groups of the copper grating electrode alternately connected electrically, and the specific fabrication process can be found in the [Experimental procedures](#). Due to the novel design of the rotor structure, the fabricated 3D-printed shared rotor was clearly tiny in size (diameter of 70 mm), flat (height of 3.6 mm), and light in weight (weight of 22 g). Meanwhile, the diameter of the PTFE rollers was 6 mm, which was larger than the thickness of the bearing structure turntable, so two BS-TENG units were integrated into one acrylic tube through two stators that were distributed on both sides of the rotor, forming a double-BS-TENGs.

By coupling the precise combination of PTFE material and soft sponge structure, a self-adaptable buffering function was also obtained to produce a high and stable output within the working range of 100 to 1,500 rpm. Therefore, BS-TENG can achieve effective mechanical energy harvesting by wheel rotation and realize a longer service life. The basic working mechanism of the BS-TENG is illustrated in [Figure 1E](#). The triboelectrification between the copper electrodes and the PTFE roller generates positive electrostatic charges on the copper electrodes and negative charges on the PTFE roller surface, since the electronegativity of the PTFE material is higher than that of copper ([Figure 1Ei](#)). Owing to the demonstration, part of the charge is displayed, and the total tribo-charge amounts on the copper and PTFE are equivalent. Subsequently, when the PTFE rollers separate from the left copper electrode and roll toward the right electrode, the negative charge of the PTFE roller will induce an electric flow from the right copper electrode to the left one through an external circuit ([Figure 1Eii](#)). The center of the PTFE roller totally rolls to the copper electrode on the right and thus the electric flow stops, which means that all of the positive charges are completely transferred from the left copper electrode to the right one ([Figure 1Eiii](#)). Similarly, when another PTFE roller reaches the left copper electrode, the electricity on the left copper electrode will return to the right one through an external circuit ([Figure 1Eiv](#)). According to the electrostatic induction, with the relative rotation of PTFE rollers and the copper electrode, free charges on the electrodes will be redistributed between two groups of copper electrodes through the external circuit in order for the change of potential difference to be balanced.

Electrical characterizations for the BS-TENG

In order to more accurately characterize the basic electrical output performance of the BS-TENG, a servomotor-driven rotor system with adjustable rotational speed controlled by alternating current (AC) servo driven was established. [Figure 2A](#) shows that the measured short-circuit current of BS-TENG increased linearly, with rotational speeds increasing from 100 to 1,500 rpm, which can reach 30 μA at 1,500 rpm, indicating a positively proportional relationship with rotational speed. With a different trend, open-circuit voltage and transferred charge quantity remained almost constant in the range from 500 to 1,500 rpm, and the peak-to-peak values of open-circuit voltage and transferred charge quantity maintained at about 72 V and 22 nC, respectively, as shown in [Figures 2B](#) and [2C](#). Compared with the other rotational speeds of 100 and 300 rpm, the value of open-circuit voltage and transferred charge quantity decreased to a certain extent. In the process of the device design, in order to buffer and reduce friction, a layer of soft sponge was attached to the back of the electrode. At high speeds, the contact area between the PTFE rollers and the electrode was slightly reduced due to the excessively fast speed, resulting in a slight decrease in charge and voltage. Similar experimental phenomenon can also be found in the work of Wang et al.²⁶ and Han et al.²⁷ In

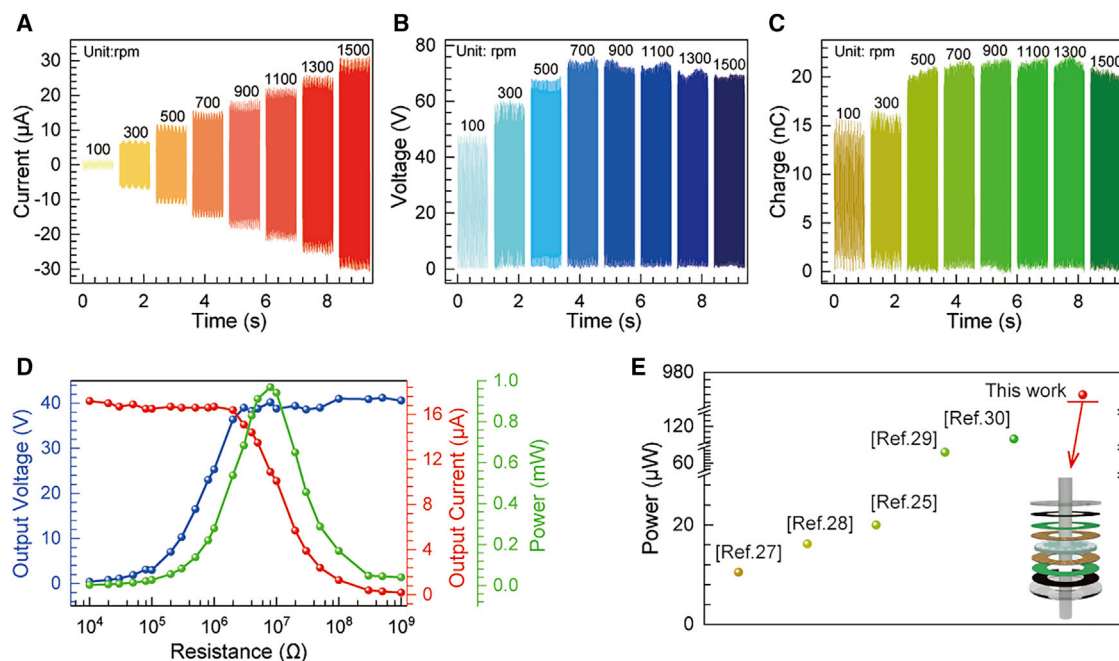


Figure 2. Basic output characteristics of the BS-TENG

(A–C) Effects of the motor rotational speed in range of 100 to 1,500 rpm on (A) output current, (B) output voltage, and (C) transferred charge of the TENG. (D) Measured output current, voltage, and calculated power on different external loading resistances at the rotational speed of 600 rpm. (E) Compare the peak power of the present TENGs.

In addition, the stability of the BS-TENG running at high speeds was tested, as shown in Figure S1A. The open voltage stabilized at 73 V after continuous operation for 10,000 cycles at 900 rpm, implying the excellent output ability of the BS-TENG. The waveform diagram at the beginning and end of the test was enlarged, and the waveform and size were almost unchanged, as can be seen from the illustration of Figure S1A. Thus, BS-TENG enabled high reliability as an energy harvester and sensing device. The electrode disk and PTFE ball were compared before and after the stability test, and the surface morphology was basically changed (Figure S1B).

In order to investigate basic properties and influences of related parameters, the schematic model of BS-TENG was designed, and a detailed explanation can be obtained from Note S1. The short-circuit current (I_{sc}) is the transferred charge quantity (Q_{sc}) divided by rolling time, which can be shown as:

$$I_{sc} = \frac{Q_{sc}}{w/v} \quad (1)$$

In this equation, v is velocity of the PTFE rollers. From the basic relationship between V_{oc} , Q_{sc} , and C ,²⁸ V_{oc} can be easily obtained as following equation:

$$V_{oc} = \frac{Q_{sc}}{C}, \quad (2)$$

where V_{oc} is the output voltage, and C stands for capacitance. According to the theory of the rolling-type free-standing mode TENG, the BS-TENG can be regarded as an almost constant capacitor.²⁸ As can be seen from Equations 1, 2, and S5 (Note S1), as v is increasing, I_{sc} is increasing, while V_{oc} does not change, which, due to the transferred charges, is constant.

For a superior application in mechanical energy harvesting, BS-TENG was tested at a rotational speed of 600 rpm with external load resistances from 0.01 to 100 M Ω . [Figure 2D](#) shows the result that currents remained unchanged until the load resistance increased to 2 M Ω . Subsequently, the measured current dropped sharply in the range of 2 and 100 M Ω . Conversely, the output voltage remained unchanged when the unit load resistance increased to 0.1 M Ω , then the measured output voltage increased rapidly in the range of 0.1 to 3 M Ω and kept stable after 3 M Ω . Consequently, the instantaneous power was maximized at a load resistance of 8 M Ω , which corresponded to a peak power of 0.96 mW. The power density was also calculated, and it delivers a maximum power density of 7.62 W/m³ ([Figure S2](#)). The peak power of the BS-TENG in this work was compared with previous roller-structure and turntable-structure TENGs, as shown in [Figure 2E](#). The power generated by the BS-TENG was much greater than the power of 10.5 μ W, 16.2 μ W, 20 μ W, 74 μ W, and 111 μ W in the work of Li et al.,²⁹ Choi et al.,³⁰ Han et al.,²⁷ Lin et al.,³¹ and Yang et al.,³² respectively. In addition, to verify the characteristics of the BS-TENG with broadband response to rotational speed to harvest rotational energy, the working scope of BS-TENG was 100 to 1,500 rpm compared with previous representative works, which are mentioned above. However, the maximum speed at which their TENGs worked stably was basically at 1,000 rpm, which indicates that our BS-TENG has superior performance for wide speed-range rotational energy harvesting. Therefore, these works are difficult to meet stable output at high speeds. Herein, the novel and precise structure of the BS-TENG was obtained so that rollers could slide with full contact and low friction to achieve a superior performance output at high rotational speeds. In order to verify the influence of the external environment on the performance of the BS-TENG, we added an experiment to measure the voltage signal of BS-TENG at room temperature (20°C), 40°C, and 60°C. The environments of 40°C and 60°C were simulated with a hot air blower. We could clearly see that different temperatures have basically no effect on the output of the BS-TENG. ([Figure S3A](#)). In order to verify the impact of vehicle braking on the performance of the BS-TENG when the generator was integrated into the vehicle, we suddenly increased and decreased the speed to simulate the actual driving conditions of the vehicle. It can be seen from the results that the BS-TENG can have a good output performance when the speed is suddenly increased and decreased ([Figure S3B](#)).

Compared with the traditional manufacturing industry, which manufactures the devices with complex structures and high costs, 3D printing has the advantage of materials saving, high precision, and simple preparation. Thus, no matter what kind of device we want, it can be 3D-printed to meet the application of the industrial manufacturing field. Here, BS-TENGs with different lengths, different numbers of balls, and different structures were produced by 3D printing. The photograph of BS-TENGs with different lengths (7 mm, 8 mm, 9 mm, 10 mm, and 11 mm) of rollers can be seen in [Figure S4](#). Notably, in order to eliminate the huge disparities in linear velocity caused by the large difference between the inner and outer radius of the ball in circular motion ([Note S2](#)), the measure of 10-mm rollers was composed of double 5-mm rollers, and 11-mm rollers were made up of 5 mm and 6 mm rollers, respectively. [Figure 3A](#) shows a 3D graph of a short-circuit current with different lengths of rollers and rotational speeds from 100 to 1,500 rpm. In [Figure S5A](#), the 2D graph gives a clear view that a few changes of short-circuit currents with different lengths of rollers while rotational speed affect vastly. Meanwhile, an intuitive view of the increasing short-circuit current with a rotational growth can also be seen. The open-circuit voltage of different lengths of rollers decreased, to a certain extent, at a low speed, which remained almost constant in the range from 500 to 1,500 rpm, as shown in [Figure 3B](#). On the other hand, the open-circuit

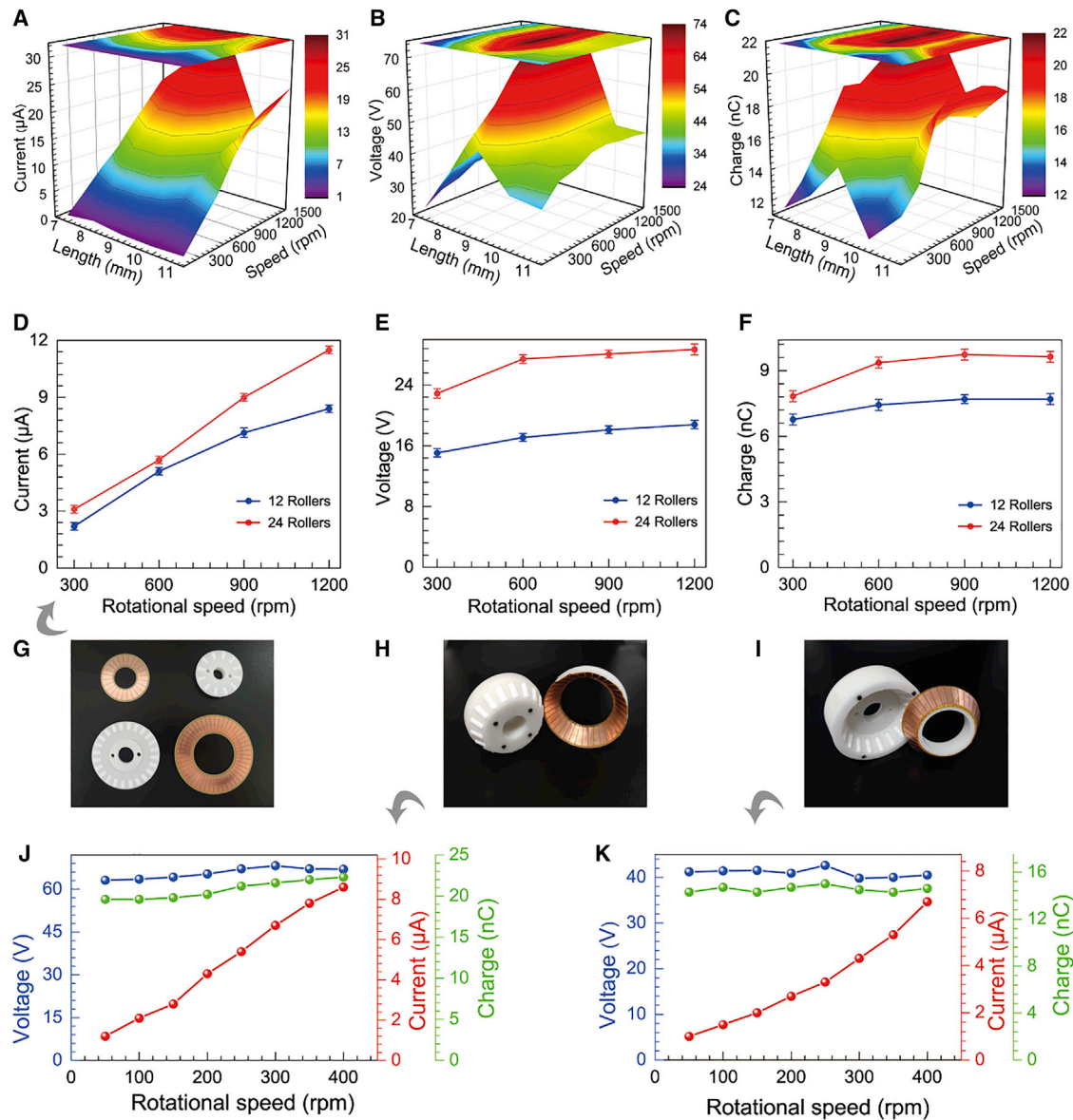


Figure 3. Systematic discussion of the advantages of 3D printed BS-TENGs

(A–C) 3D surface graphs show the effects of length of rollers and motor rotational speed in range of 100 to 1,500 rpm on (A) output current, (B) output voltage, and (C) transferred charge of BS-TENG.

(D–F) Comparison of the current, voltage, and charge for BS-TENG with different numbers of rollers. The error bars can be defined as the standard deviation calculated by testing the current, voltage, and charge of three parallel measurements for each device.

(G) The photograph of BS-TENG with different numbers of rollers.

(H) The photograph of the convex-tapered roller BS-TENG.

(I) The photograph of the concave-tapered roller BS-TENG.

(J and K) The electrical output of convex-tapered roller BS-TENG (J) and the electrical output of concave-tapered roller BS-TENG (K).

voltage was less affected by the rotational speed, and it was more affected by the length of the balls, as the curves presented in Figure S5B show. Similarly, the transferred charge follows the same trend with the open-circuit voltage (Figure 3C; Figure S5C). According to Equation 5 in Note S1, the transferred charge cannot be affected.

Next, two 3D-printed shared rotors with 12 and 24 rollers were produced by 3D printing, and two types of electrodes corresponding to the two rotors were obtained

through PCB technology, as indicated in the photograph of [Figure 3G](#). As shown in [Figures 3D–3F](#), the increased short-circuit current with a rotational speed growth, stable open-circuit voltage, and stable transferred charges at 300 to 1,200 rpm, respectively. In order to give further expression to advantages and convenience of 3D printing, the convex-tapered roller-bearing structure TENG ([Figure 3H](#)) and the concave-tapered roller-bearing structure TENG ([Figure 3I](#)) were designed. As the rotational speed increased from 50 to 400 rpm, the peak-to-peak value of the open-circuit voltage and the peak value of transferred charge quantity of the convex-tapered roller-bearing structure TENG remained steady at around 67 V and 21 nC, respectively, while the peak value of the short-circuit current increased almost linearly with the rotational speed, reaching up to 8.6 μA at the rotational speed of 400 rpm, as shown in [Figure 3J](#). Within the same speed range, the voltage and the transferred charge quantity of the concave-tapered roller-bearing structure TENG stayed around 41 V and 14.5 nC, respectively, while the peak value of the short-circuit current increased up to 6.7 μA at 400 rpm, as presented in [Figure 3K](#). Therefore, BS-TENG obtained by 3D printing was demonstrated as remarkably stable at varying speeds, with negligible output changes, which is the basis for rotating mechanical energy harvesting.

As mentioned earlier, the 3D-printed shared rotor of BS-TENG was only 3.6 mm, which means that multiple BS-TENGs can be arrayed without a significant increase in size. To improve the power output and optimize the structure design, a SVPM system was developed based on the eight integrated BS-TENG units, which play dual roles as a BS-TENG's energy-harvesting network and a self-powered sensing system for vehicle temperature and speed monitoring, as systematically shown in [Figure S6A](#). A sensing system was obtained by a BS-TENG unit, and the BS-TENG's energy-harvesting network was formed by connecting seven BS-TENG units in parallel. The specific assembly flow chart of the SVPM system can be seen in [Figures S6B–S6F](#). The middle gear fixed on the shaft acted as the driving gear, and the other four gears were uniformly distributed around the middle one as the driven gears ([Figure S6D](#)). The photographs of double-BS-TENGs with two views are shown in [Figures 3G and 3H](#).

With the advantages of being small, flat, and light in weight, multiple BS-TENGs can be arrayed, as shown in [Figure 4A](#). The short-circuit current and transferred charges of the BS-TENG's energy-harvesting network with different numbers of BS-TENG units are presented in [Figures 4B and 4C](#), respectively. As can be observed, with an increasing number of units, the peak value of short-circuit current increased from 12 μA to 76 μA , and transferred charges increased from 12 nC to 85 nC in an almost linear way at 900 rpm. To visually investigate the relationship between the electric outputs of seven BS-TENG units in parallel and the rotational speed, a systematical measurement was performed under different rotational speeds varying from 100 to 1,500 rpm, as shown in [Figure 4D](#). With the increasing rotational speeds, the short-circuit current increased linearly up to 112 μA at 1,500 rpm. The stable open-circuit voltage of almost 80 V and the constant transferred charges of 85 nC were measured in the range of 100 to 1,500 rpm. This means that after multiple BS-TENG arrays, the SPVM-system can still maintain stable operation at up to 1,500 rpm and have good performance output. The system provides a potential strategy for the future development of an intelligent automated vehicle.

To investigate the charging performance of the BS-TENG's energy-harvesting network, a simple power management circuit was designed. Using seven rectifier bridges, the alternate voltage from seven BS-TENGs was rectified to the direct

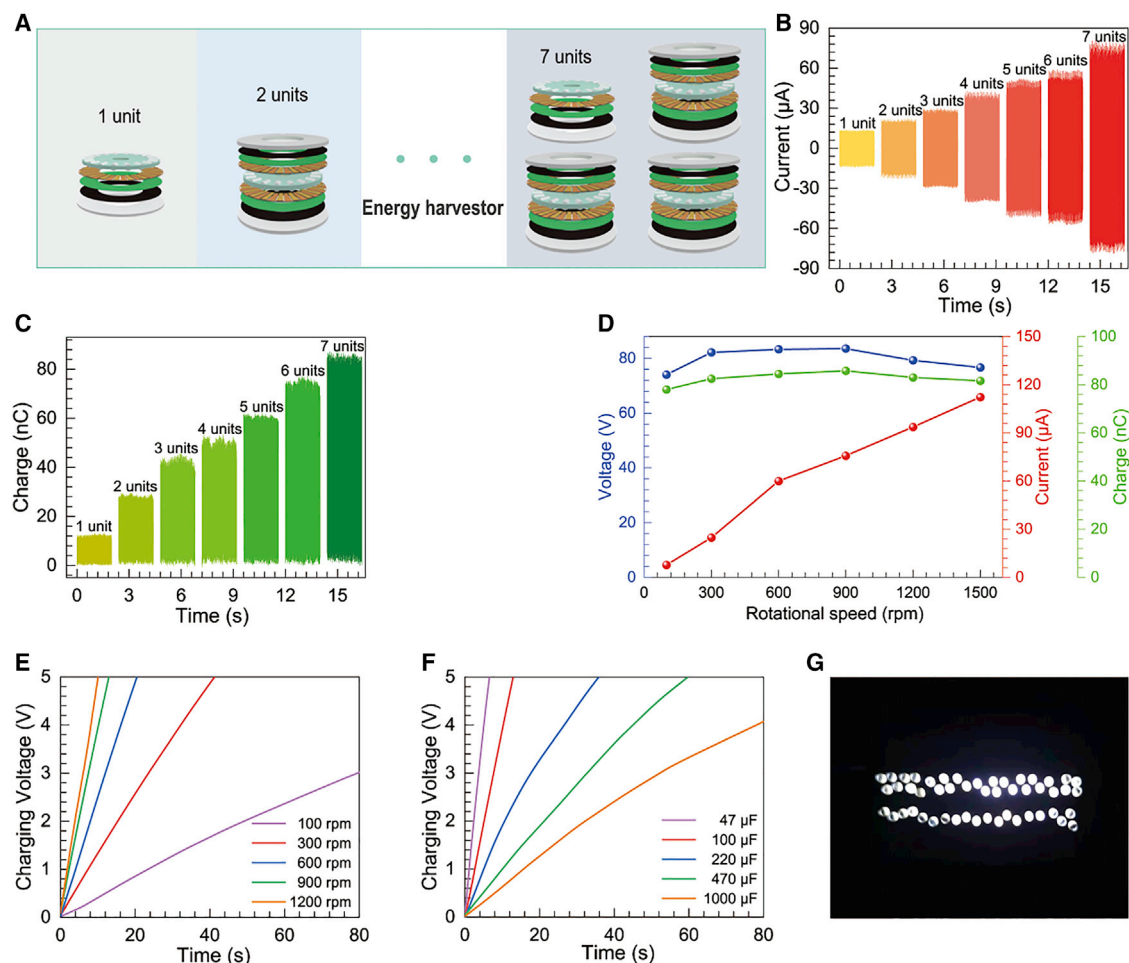


Figure 4. Demonstrations of BS-TENG array with good electrical output and self-powering capability of the self-powered vehicle monitoring system

(A) Schematic illustration of integrated BS-TENGs network.

(B and C) The current (B) and the charge (C) increases linearly while increasing the number of the BS-TENGs.

(D) The output of seven BS-TENGs connected in parallel under different rotational speed.

(E) 100- μ F charging of capacitor by the BS-TENG's energy harvesting network at different rotational speeds of the motor.

(F) Charging voltage on various capacitors for the BS-TENG's energy harvesting network at 600 rpm.

(G) Photograph of 50 LEDs lit directly by the network.

current voltage, and then a capacitor was charged in parallel. Figure 4E shows the charging voltage curve of a 100 μ F capacitor by the BS-TENG's energy-harvesting network at a rotational speed of 100 to 1,200 rpm. The capacitor was charged from empty to 5 V within 20 s at 600 rpm. The charging performance of the BS-TENG's energy-harvesting network for different capacitors was also observed. Figure 4F compares the voltage curves of 47, 100, 220, 470, and 1000 μ F capacitors charged by the BS-TENG's energy-harvesting network. The 470 μ F capacitor was charged to 5 V in 60 s, and the 1,000 μ F capacitor was charged to 4 V in 80 s. In addition, in order to intuitively demonstrate the capability of the BS-TENG's energy-harvesting network as an energy harvester and power source, 50 LEDs were lit up simultaneously by it, as shown in the snapshot of Figure 4G (see Video S1).

Application of BS-TENG for rotational energy harvesting

In order to demonstrate the applications of the BS-TENG in rotational energy harvesting, an environment that the rotation of the servomotor simulates the rotation

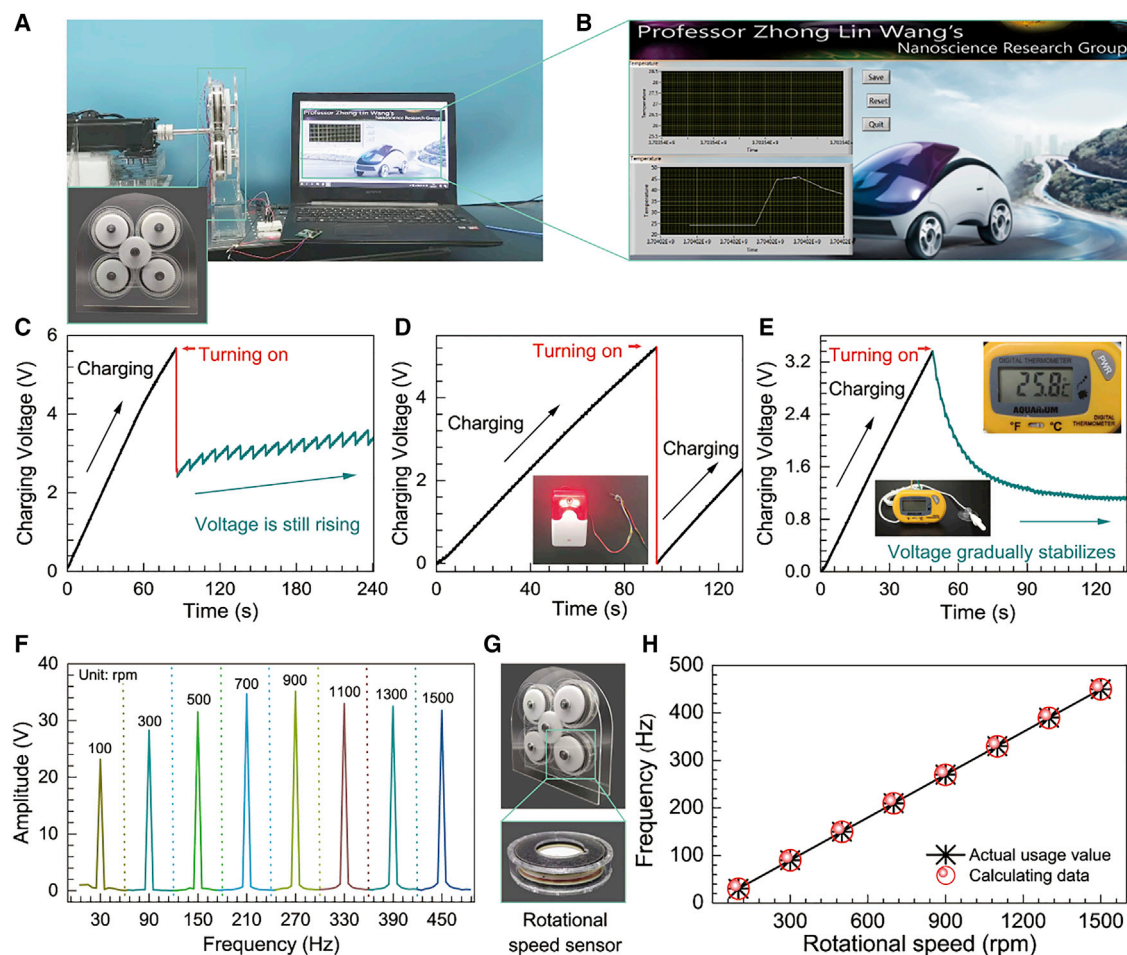


Figure 5. Application demonstrations of the self-powered vehicle monitoring system based on BS-TENGs

- (A) Application of BS-TENG's energy harvesting network powering a wireless temperature sensor.
 (B) The interface of self-powered temperature monitoring system.
 (C) Charging process for a capacitor of $470\ \mu\text{F}$ to continuously power the wireless temperature sensor.
 (D) Voltage profile on the capacitor charged by the BS-TENG's energy harvesting network to power the alarm. The inset is the photograph of the alarm while driving.
 (E) Voltage profile for continuously monitoring the ambient temperature. The insets illustrate the states of continuous monitoring.
 (F) Characteristic frequency analysis of BS-TENG.
 (G) One BS-TENG unit in self-powered vehicle monitoring system is used as a rotational speed sensor.
 (H) Calculated rotational speed of BS-TENG at different signal frequencies.

of wheels was established in the laboratory. Figure 5A shows a photograph of a SVPM system and the test scenario of the BS-TENG's energy-harvesting network powering a temperature sensor. The temperature of wheels on vehicles is particularly important for automotive safety systems. Hence, it is imperative that a powered real-time temperature monitoring system was developed, including the capacitor, sensor, signal transmitter, and a signal receiver (Figure S7A). The enlarged view of the temperature monitoring interface and the whole process is presented in Figure 5B. A capacitor of $470\ \mu\text{F}$ was used as an energy storage and to power the temperature monitoring system because it cannot be directly powered by the TENG. In this system, the temperature sensor can transmit the temperature signals to the signal receiver, and the temperature value will be displayed on the computer in real time by signal processing (Figure S7B). The charging curve of the capacitors as the system operates is shown in Figure 5C. First, the capacitor was charged to

5.5 V in 85 s, then the temperature monitoring system was turned on by a processing circuit. The stored electrical energy allowed the temperature monitoring system to function normally, and the temperature value of the environment was measured as 24.1°C. Subsequently, the voltage of the capacitor increased slowly and gradually tended to be stable, which enabled real-time self-powered temperature monitoring. Similarly, the capacitor was charged to 4.6 V, then the alarm was triggered by the processing circuit, as shown in [Figure 5D](#) (see [Video S2](#)). In terms of future research trends and the artificial intelligence industry of concern, it is completely possible to integrate a real-time, self-powered, temperature-monitoring warning system into an artificial intelligence automated vehicle, realizing a miniaturized energy collector and an intelligent system based on the TENG. In addition, the energy-harvesting network can also harvest the rotational energy to power the thermometer to continuously monitor the temperature, as illustrated in [Figure 5E](#) (see [Video S3](#)).

Significantly, the BS-TENG with regular waveform was also utilized as a wheel speed sensor^{33–35} ([Figure S8](#)). To obtain the actual characteristic frequency, it was necessary to perform fast Fourier transform (FFT) on the output signal.³⁶ Through FFT, the time domain signal could be converted rapidly to a frequency domain signal, and the characteristic frequency of the signal could be extracted. The accuracy of the characteristic frequency depended on the number of complete cycles in the sampling time. The set sampling time and sampling rate should be guaranteed to have a sufficient measurement accuracy. Notably, too short a sampling time made the characteristic frequency far from the true value, while too long a sampling time was not conducive to real-time calculations and reduced the processing efficiency.³⁷ The sampling rate was also an important factor to ensure the accuracy of the characteristic frequency. Therefore, to balance the accuracy and efficiency, the sampling time of 0.6 s and sampling rate of 10,000 were chosen. [Figure 5F](#) shows the results of FFT analysis from 100 to 1,500 rpm. One BS-TENG unit in the SVPM system as used as a rotational speed sensor, as shown in [Figure 5G](#). The amplitude characteristics of the corresponding characteristic frequencies were obvious, which confirms that the BS-TENG has a distinct and stable periodic output. The relationship between the characteristic (output) frequency (f) of the BS-TENG and the rotational speed of the rotor can be expressed by the following equation:

$$f = \frac{3v}{\theta}, \quad (3)$$

where v is the rotation rate (rpm) of the rotor, and θ is the center angle (°) of a single electrode grating. Here, θ for the single electrode grating is 10°. The detailed description can be seen in [Note S3](#). To understand the sensing characteristics of BS-TENG, the characteristic frequencies at different rotational speeds were extracted. According to the Equation 3, the calculated rotational speed can be obtained. The calculating data almost fall on the theoretical reference line and show a terrific match with actual rotation speed, as shown in [Figure 5H](#). For a measured speed of 100 to 1,500 rpm, the accuracy could be accurately measured to more than 99%. Detailed data can be found in [Table S1](#). As a consequence, the BS-TENG not only acts as an energy harvester and a power source but also a wheel speed sensor with high sensitivity.

This work demonstrates unique advantages and practicability of the newly developed BS-TENG for harvesting high-speed rotational energy and a self-powered sensing system, which achieved a speed breakthrough of nearly 1,500 rpm for the first time by 3D printing the diversified design in order to enable even higher working frequency. The integrated BS-TENG's network can be utilized as both a

rotational energy harvester and a self-powered high-speed sensing system for vehicle temperature and real-time speed monitoring. It was vital that one unit delivered a peak power of 0.96 mW under an external load of 8 M Ω and the rotational speed of 600 rpm. Meanwhile, a SVPM system was established by integrating eight BS-TENG units, which included a high rotational speed sensor composed of one unit and an energy-harvesting network consisting of seven units, which was capable of real-time monitoring local temperature and vehicle speed. The energy-harvesting network can produce a short-circuit current of 76 μ A, an open-circuit voltage of 72 V, and the transferred charge of 85 nC under the rotational speed of 900 rpm. Moreover, a capacitor of 1,000 μ F was charged by an integrated energy harvester to achieve a voltage of 4 V that takes nearly 80 s at 600 rpm. It could also directly light up 50 commercial LEDs and an electronic thermometer. Additionally, findings reveal that the working frequency of the BS-TENG accurately changes with the increase of rotational speed, showing its potential application as a self-powered speed sensor. Furthermore, the results confirmed that the accuracy of the self-powered vehicle speed monitoring could reach more than 99% under a wide range of 100 to 1,500 rpm, thereby indicating that the design of the BS-TENG is reliable for practical applications. Therefore, the BS-TENG implies that a breakthrough has been made for rotational energy harvesting and the self-powered sensing system under a high rotational speed. Our work not only shows a new approach for upgrading the working frequency of TENGs and electrical output performances but also provides new opportunities for utilizing wasted rotational energy and multifunctional self-powered sensing and demonstrates potential applications in an intelligent vehicle autonomous driving system.

EXPERIMENTAL PROCEDURES

Resource availability

Lead contact

Further information and requests for resources and reagents should be directed to and will be fulfilled by the lead contact, Baodong Chen (chenbaodong@binn.cas.cn).

Materials availability

This study did not generate new unique reagents.

Data and code availability

- All of the data reported in this article will be shared by the lead contact upon request.
- This article does not report original code.

Fabrication of the BS-TENG and the self-powered system

First, two acrylic plates are used as the framework of the device, each of which contained five round holes with a diameter of 18 mm for mounting bearings. Next, a 5-mm thick sponge and a 2-mm thick acrylic plate were both cut into two discs with the same inner diameter of 42 mm and different out diameters of 72 mm and 90 mm, respectively. The height, inner diameter, and outer diameter of the acrylic tube were 16 mm, 80 mm, and 90 mm respectively. Those processes were operated by laser cutting machines. Then, 6-mm PTFE rollers with different lengths, four shafts with a length of 6 cm and a shaft with a length of 12 cm, and gears were obtained by lathe machining.

For the rotor, the turntable of cylindrical roller with the interspaces that were left was obtained by 3D-printed technology, and then PTFE rollers were filled into the interspaces. For the electrode disk, the epoxy glass fiber substrate with copper layers (thickness of 35 μ m) was fabricated by the PCB technique. The patterned copper sectors were

divided into two groups, each of which contained 18 grating electrodes. Each sector electrode's inner diameter was 42 mm and the out diameter was 72 mm, with an angle of 10°. In other words, the disc was separated into 36 parts. For the stator, the copper electrode disk with two groups of complementary electrodes, which were electrically connected, was pasted on the sponge and then stuck with the acrylic substrate. Therefore, one BS-TENG unit was obtained through a combination of a rotor and a stator. Two BS-TENG units are obtained by encapsulating two electrode disks and a rotor into an acrylic tube. By that analogy, eight BS-TENGs were built and fixed by four acrylic tubes, forming four double-BS-TENGs. Combining those parts mentioned above, the SVPM system was fabricated, which consisted of four double-BS-TENGs containing eight BS-TENG units, two acrylic plates, and five gears.

The 6-cm shaft was connected to the rotor. Each shaft was connected to the gears and fixed on the framework of the acrylic plate. Note that the 12-cm shaft was linked to the middle gear and the servomotor as a transmission device. Four rotors were fixed on the shafts and directly driven by the driving gear to rotate, while the electrode disks were locked on the acrylic tubes, which were fixed on the frame of the acrylic plate.

Characterization

The electric output signal of the BS-TENG device was measured under the ideal triggering generated by servomotor triggering. The short-circuit current, the open-circuit voltage, and the transferred charge were measured by a Keithley 6517 system electrometer. The software platform was constructed based on LabVIEW, which can achieve real-time data acquisition and analysis.

SUPPLEMENTAL INFORMATION

Supplemental information can be found online at <https://doi.org/10.1016/j.xcrp.2021.100666>.

ACKNOWLEDGMENTS

The authors acknowledge support from the Natural Science Foundation of Beijing Municipality (grant 2192062), which was supported by the National Natural Science Foundation of China (grants 51502147, 51702018, and 11704032). The research was sponsored by the National Key R & D Project from the Minister of Science and Technology (2016YFA0202704) and the Beijing Municipal Science and Technology Commission (Z181100003818016 and Y3993113DF).

AUTHOR CONTRIBUTIONS

Methodology, data curation, investigation, and writing – original draft preparation, J.Y.; investigation and visualization, Y.S.; formal analysis and resources, J.Z.; writing – review & editing, supervision, and resources, B.C.; conceptualization, supervision, and writing - review & editing, Z.L.W.

DECLARATION OF INTERESTS

The authors declare no competing interests.

Received: August 5, 2021

Revised: September 22, 2021

Accepted: November 5, 2021

Published: November 22, 2021

REFERENCES

- Wang, Z.L., Chen, J., and Lin, L. (2015). Progress in triboelectric nanogenerators as a new energy technology and self-powered sensors. *Energy Environ. Sci.* 8, 2250–2282.
- Wang, Z.L., Jiang, T., and Xu, L. (2017). Toward the blue energy dream by triboelectric nanogenerator networks. *Nano Energy* 39, 9–23.
- He, Y., Chang, Z., Wu, S., and Zhou, H. (2018). Effective strategies for long-cycle life lithium–sulfur batteries. *J. Mater. Chem. A Mater. Energy Sustain.* 6, 6155–6182.
- Nam, S.M., and Kim, H.J. (2021). WSN-SES/MB: System Entity Structure and Model Base Framework for Large-Scale Wireless Sensor Networks. *Sensors (Basel)* 21, 430.
- Zhang, B., Chen, J., Jin, L., Deng, W., Zhang, L., Zhang, H., Zhu, M., Yang, W., and Wang, Z.L. (2016). Rotating-Disk-Based Hybridized Electromagnetic-Triboelectric Nanogenerator for Sustainably Powering Wireless Traffic Volume Sensors. *ACS Nano* 10, 6241–6247.
- Xu, S., Liu, W., Hu, B., and Wang, X. (2019). Circuit-integratable high-frequency micro supercapacitors with filter/oscillator demonstrations. *Nano Energy* 58, 803–810.
- Liu, F., Wang, Z., Zhang, H., Jin, L., Chu, X., Gu, B., Huang, H., and Yang, W. (2019). Nitrogen, oxygen and sulfur co-doped hierarchical porous carbons toward high-performance supercapacitors by direct pyrolysis of kraft lignin. *Carbon* 149, 105–116.
- Wang, Z.L. (2019). Entropy theory of distributed energy for internet of things. *Nano Energy* 58, 669–672.
- Chen, X., Gao, L., Chen, J., Lu, S., Zhou, H., Wang, T., Wang, A., Zhang, Z., Guo, S., Mu, X., et al. (2020). A chaotic pendulum triboelectric-electromagnetic hybridized nanogenerator for wave energy scavenging and self-powered wireless sensing system. *Nano Energy* 69, 104440.
- Liang, X., Jiang, T., Liu, G., Feng, Y., Zhang, C., and Wang, Z.L. (2020). Spherical triboelectric nanogenerator integrated with power management module for harvesting multidirectional water wave energy. *Energy Environ. Sci.* 13, 277–285.
- Tian, J., Chen, X., and Wang, Z.L. (2020). Environmental energy harvesting based on triboelectric nanogenerators. *Nanotechnology* 31, 242001.
- Wang, Z.L., and Song, J.H. (2006). Piezoelectric nanogenerators based on zinc oxide nanowire arrays. *Science* 312, 242–246.
- Fan, F.-R., Tian, Z.-Q., and Wang, Z.L. (2012). Flexible triboelectric generator. *Nano Energy* 1, 328–334.
- Ren, Z., Wang, Z., Liu, Z., Wang, L., Guo, H., Li, L., Li, S., Chen, X., Tang, W., and Wang, Z.L. (2020). Energy Harvesting from Breeze Wind (0.7–6 m s⁻¹) Using Ultra-Stretchable Triboelectric Nanogenerator. *Adv. Energy Mater.* 10, 2001770.
- Wang, Y., Yu, X., Yin, M., Wang, J., Gao, Q., Yu, Y., Cheng, T., and Wang, Z.L. (2021). Gravity triboelectric nanogenerator for the steady harvesting of natural wind energy. *Nano Energy* 82, 105740.
- Han, K., Luo, J., Feng, Y., Xu, L., Tang, W., and Wang, Z.L. (2020). Self-powered electrocatalytic ammonia synthesis directly from air as driven by dual triboelectric nanogenerators. *Energy Environ. Sci.* 13, 2450–2458.
- Guo, T., Liu, G., Pang, Y., Wu, B., Xi, F., Zhao, J., Bu, T., Fu, X., Li, X., Zhang, C., and Wang, Z.L. (2018). Compressible hexagonal-structured triboelectric nanogenerators for harvesting tire rotation energy. *Extreme Mech. Lett.* 18, 1–8.
- Xie, Z., Zeng, Z., Wang, Y., Yang, W., Xu, Y., Lu, X., Cheng, T., Zhao, H., and Wang, Z.L. (2020). Novel sweep-type triboelectric nanogenerator utilizing single freewheel for random triggering motion energy harvesting and driver habits monitoring. *Nano Energy* 68, 104360.
- Zhang, D., Wang, D., Xu, Z., Zhang, X., Yang, Y., Guo, J., Zhang, B., and Zhao, W. (2021). Diversiform sensors and sensing systems driven by triboelectric and piezoelectric nanogenerators. *Coord. Chem. Rev.* 427, 213597.
- Zhong, W., Xu, L., Zhan, F., Wang, H., Wang, F., and Wang, Z.L. (2020). Dripping Channel Based Liquid Triboelectric Nanogenerators for Energy Harvesting and Sensing. *ACS Nano* 14, 10510–10517.
- Chen, B., Tang, W., Jiang, T., Zhu, L., Chen, X., He, C., Xu, L., Guo, H., Lin, P., Li, D., et al. (2018). Three-dimensional ultraflexible triboelectric nanogenerator made by 3D printing. *Nano Energy* 45, 380–389.
- Gao, S., Zhu, Y., Chen, Y., Tian, M., Yang, Y., Jiang, T., and Wang, Z.L. (2019). Self-power electroreduction of N₂ into NH₃ by 3D printed triboelectric nanogenerators. *Mater. Today* 28, 17–24.
- Zhang, C., Liu, L., Zhou, L., Yin, X., Wei, X., Hu, Y., Liu, Y., Chen, S., Wang, J., and Wang, Z.L. (2020). Self-Powered Sensor for Quantifying Ocean Surface Water Waves Based on Triboelectric Nanogenerator. *ACS Nano* 14, 7092–7100.
- Li, S., Liu, D., Zhao, Z., Zhou, L., Yin, X., Li, X., Gao, Y., Zhang, C., Zhang, Q., Wang, J., and Wang, Z.L. (2020). A Fully Self-Powered Vibration Monitoring System Driven by Dual-Mode Triboelectric Nanogenerators. *ACS Nano* 14, 2475–2482.
- Wang, Z., An, J., Nie, J., Luo, J., Shao, J., Jiang, T., Chen, B., Tang, W., and Wang, Z.L. (2020). A Self-Powered Angle Sensor at Nanoradian Resolution for Robotic Arms and Personalized Medicare. *Adv. Mater.* 32, e2001466.
- Wang, J., Ding, W., Pan, L., Wu, C., Yu, H., Yang, L., Liao, R., and Wang, Z.L. (2018). Self-Powered Wind Sensor System for Detecting Wind Speed and Direction Based on a Triboelectric Nanogenerator. *ACS Nano* 12, 3954–3963.
- Han, Q., Ding, Z., Qin, Z., Wang, T., Xu, X., and Chu, F. (2020). A triboelectric rolling ball bearing with self-powering and self-sensing capabilities. *Nano Energy* 67, 104277.
- Niu, S., Liu, Y., Chen, X., Wang, S., Zhou, Y.S., Lin, L., Xie, Y., and Wang, Z.L. (2015). Theory of freestanding triboelectric-layer-based nanogenerators. *Nano Energy* 12, 760–774.
- Li, X.H., Han, C.B., Jiang, T., Zhang, C., and Wang, Z.L. (2016). A ball-bearing structured triboelectric nanogenerator for nondestructive damage and rotating speed measurement. *Nanotechnology* 27, 085401.
- Choi, D., Sung, T., and Kwon, J.Y. (2018). A Self-Powered Smart Roller-Bearing Based on a Triboelectric Nanogenerator for Measurement of Rotation Movement. *Adv. Mater. Technol.* 3, 1800219.
- Lin, Z., Zhang, B., Zou, H., Wu, Z., Guo, H., Zhang, Y., Yang, J., and Wang, Z.L. (2020). Rationally designed rotation triboelectric nanogenerators with much extended lifetime and durability. *Nano Energy* 68, 104378.
- Yang, H., Liu, W., Xi, Y., Lai, M., Guo, H., Liu, G., Wang, M., Li, T., Ji, X., and Li, X. (2018). Rolling friction contact-separation mode hybrid triboelectric nanogenerator for mechanical energy harvesting and self-powered multifunctional sensors. *Nano Energy* 47, 539–546.
- Wu, Z., Zhang, B., Zou, H., Lin, Z., Liu, G., and Wang, Z.L. (2019). Multifunctional Sensor Based on Translational-Rotary Triboelectric Nanogenerator. *Adv. Energy Mater.* 9, 1901124.
- Wang, Z.L. (2020). Triboelectric Nanogenerator (TEG)—Sparking an Energy and Sensor Revolution. *Adv. Energy Mater.* 10, 2000137.
- Yin, X., Liu, D., Zhou, L., Li, X., Xu, G., Liu, L., Li, S., Zhang, C., Wang, J., and Wang, Z.L. (2020). A Motion Vector Sensor via Direct-Current Triboelectric Nanogenerator. *Adv. Funct. Mater.* 30, 2002547.
- Jin, L., Zhang, S.L., Xu, S., Guo, H., Yang, W., and Wang, Z.L. (2021). Free-Fixed Rotational Triboelectric Nanogenerator for Self-Powered Real-Time Wheel Monitoring. *Adv. Mater. Technol.* 6, 2000918.
- Xie, Z., Dong, J., Li, Y., Gu, L., Song, B., Cheng, T., and Wang, Z.L. (2020). Triboelectric rotational speed sensor integrated into a bearing: A solid step to industrial application. *Extreme Mech. Lett.* 34, 100595.